Although the specific locations used in these tests varied between subjects, 3–6 of the same questions on each test were administered to E.P. and at least four of the five controls. In addition, the 'familiar navigation' and 'novel navigation' tasks were matched across subjects with respect to the distance travelled (mean, 3.0 and 3.3 miles, respectively) and the number of turns needed (mean, 3.0 and 2.7 turns, respectively) to reach each destination. The routes that subjects reported in the verbal navigation tasks were scored as correct if they incorporated the correct sequence and direction of turns necessary to reach the destination. All subjects typically reported street names as they navigated their routes. However, presumably because of his anomia (Boston Naming Test score, 42; maximum score, 60, mean of four control subjects, 54.5)[7], E.P. omitted street names more frequently than did the control subjects (0.5 omissions per question compared with 0.3 omissions for controls; range, 0.1–0.5). Accordingly, we also used another scoring method, which required both a correct sequence of turns and correct street names. An independent scorer who was blind to subject identity scored all transcripts using both scoring criteria. Average inter-scorer reliability across both scoring criteria was 0.91.

The five verbal navigation questions for current neighbourhoods were administered in the same way as the 'familiar navigation' task. Across subjects, the questions were similar with respect to the distance travelled and the number of turns needed to reach location (mean, 6.5 miles and 5.5 turns, respectively).

Received 29 April; accepted 9 June 1999.

1. Scoville, W. B. & Milner, B. Loss of recent memory after bilateral hippocampal lesions. *J. Neurol. Neurosurg. Psychiat.* **20,** 11–21 (1957).
2. Mishkin, M. Memory in monkeys severely impaired by combined but not separate removal of the amygdala and hippocampus. *Nature* **273,** 297–298 (1978).
3. Squire, L. R. Memory and the hippocampus: a synthesis from findings with rats, monkeys, and humans. *Psychol. Rev.* **99,** 195–231 (1992).
4. O'Keefe, J. & Nadel, L. *The Hippocampus as a Cognitive Map* (Clarendon, Oxford, 1978).
5. Jarrard, L. E. What does the hippocampus really do? *Behav. Brain Res.* **71,** 1–10 (1995).
6. Cohen, N. J. & Eichenbaum, H. *Memory, Amnesia, and the Hippocampal System* (MIT Press, Cambridge, Massachusetts, 1993).
7. Reed, J. M. & Squire, L. R. Retrograde amnesia for facts and events: Findings from four new cases. *J. Neurosci.* **18,** 3943–3954 (1998).
8. Hamann, S. B. & Squire, L. R. Intact perceptual memory in the absence of conscious memory. *Behav. Neurosci.* **111,** 850–854 (1997).
9. Reed, J. M., Hamann, S. B., Stefanacci, L. & Squire, L. R. When amnesic patients perform well on recognition memory tasks. *Behav. Neurosci.* **111,** 1163–1170 (1997).
10. Batschelet, E. *Statistical Methods for the Analysis of Problems in Animal Orientation and Certain Biological Rhythms* (American Institute of Biological Sciences, Washington DC, 1965).
11. O'Keefe, J. & Dostrovsky, J. The hippocampus as a spatial map: Preliminary evidence from unit activity in the freely-moving rat. *Brain Res.* **34,** 171–175 (1971).
12. Smith, M. L. & Milner, B. The role of the right hippocampus in the recall of spatial location. *Neuropsychologia* **19,** 781–793 (1981).
13. Cave, C. B. & Squire, L. R. Equivalent impairment of spatial and nonspatial memory following damage to the human hippocampus. *Hippocampus* **1,** 329–340 (1991).
14. Maguire, E. A., Burke, T., Phillips, J. & Staunton, H. Topographical disorientation following unilateral temporal lobe lesions in humans. *Neuropsychologia* **34,** 993–1001 (1996).
15. Morris, R. G. M., Garrud, P., Rawlins, J. N. P. & O'Keefe, J. Place navigation in rats with hippocampal lesions. *Nature* **297,** 681–683 (1982).
16. Aguirre, G. K., Detre, J. A., Alsop, D. C. & D'Esposito, M. D. The parahippocampus subserves topographical learning in man. *Cereb. Cort.* **6,** 823–829 (1996).
17. Maguire, E. A., Frackowiak, R. S. J. & Frith, C. D. Learning to find your way: A role for the human hippocampal formation. *Proc. R. Soc. Lond.* **263,** 1745–1750 (1996).
18. Maguire, E. A., Frackowiak, R. S. J. & Frith, C. D. Recalling routes around London: Activation of the right hippocampus in taxi drivers. *J. Neurosci.* **17,** 7103–7110 (1997).
19. Maguire, E. A. *et al.* Knowing where and getting there: A human navigation network. *Science* **280,** 921–924 (1998).
20. Nadel, L. & Moscovitch, M. Memory consolidation, retrograde amnesia and the hippocampal complex. *Curr. Opin. Neurobiol.* **7,** 217–227 (1997).
21. De Renzi, E., Faglioni, P. & Villa, P. Topographical amnesia. *J. Neurol. Neurosurg. Psychiat.* **40,** 498–505 (1977).
22. Paterson, A. & Zangwill, O. L. A case of topographical disorientation associated with a unilateral cerebral lesion. *Brain* **68,** 188–211 (1945).
23. Levine, D. N., Warach, J. & Farah, M. Two visual systems in imagery: Dissociation of "what" and "where" in imagery disorders due to bilateral posterior cerebral lesions. *Neurology* **35,** 1010–1018 (1985).
24. Bottini, G., Cappa, S., Geminiani, G. & Sterzi, R. Topographic disorientation—a case report. *Neuropsychologia* **28,** 309–312 (1990).
25. Incisa della Rochetta, A., Cipolotti, L. & Warrington, E K. Topographical disorientation: Selective impairment of locomotor space? *Cortex* **32,** 727–735 (1996).
26. Pai, M.-C. Topographic disorientation: Two cases. *J. Formos. Med. Assoc.* **96,** 660–663 (1997).
27. Takahashi, N., Kawamura, M., Shiota, J., Kasahata, N. & Hirayama, K. Pure topographic disorientation due to right retrosplenial lesion. *Neurology* **49,** 464–469 (1997).
28. Wechsler, D. *Wechsler Memory Scale-III. Administration and Scoring Manual* (Psychological Corporation, San Antonio, Texas, 1997).

Acknowledgements. We thank J. Zouzounis, L. Stefanacci, J. Frascino and the Hayward Area Historical Society for assistance. This work was supported by the Medical Research Service of the Department of Veterans Affairs, NIMH, and the McDonnell-Pew Center for Cognitive Neuroscience.

Correspondence and requests for materials should be addressed to L.R.S. (e-mail: lsquire@ucsd.edu).

A basal ganglia pacemaker formed by the subthalamic nucleus and external globus pallidus

Dietmar Plenz* **& Stephen T. Kital**

Department of Anatomy and Neurobiology, University of Tennessee, College of Medicine, Memphis, Tennessee 38163, USA

The subthalamic nucleus of the basal ganglia (STN) is important for normal movement[1,2] as well as in movement disorders[3–5]. Lesioning[6] or deep-brain stimulation[7,8] of the STN can alleviate resting tremor in Parkinson's disease. The STN[5] and its target nuclei[9,10] display synchronized oscillatory burst discharge at low frequencies, some of which correlate with tremor, but the mechanism underlying this synchronized bursting is unknown. Here we show that the excitatory STN and inhibitory, external globus pallidus (GPe) form a feedback system that engages in synchronized bursting. In mature organotypic cortex–striatum–STN–GPe cultures, neurons in the STN and GPe spontaneously produce synchronized oscillating bursts at 0.4, 0.8 and 1.8 Hz. Pallidal lesion abolishes this bursting, whereas cortical lesion favours bursting at 0.8 Hz. Pallidal bursts, although weaker than STN bursts, were required for synchronized oscillatory burst generation by recruitment of subthalmic rebound excitation. We propose that the STN and GPe constitute a central pacemaker modulated by striatal inhibition of GPe neurons. This pacemaker could be responsible for synchronized oscillatory activity in the normal and pathological basal ganglia.

To test our proposal that the STN and GPe produce synchronized oscillatory bursts, we developed an *in vitro* model[11] in which both nuclei were co-cultured with the cortex and striatum, their main extrinsic input sources, to ensure proper maturation. The STN and GPe were obtained from rats at postnatal day 0–2 and cultured with frontomedial cortex and dorsolateral striatum. After 38 ± 1 days *in vitro* ($n = 58$ cultures), spontaneous single- and multi-unit activities were recorded from the STN and GPe with one or two extracellular electrodes.

Spontaneous activity in the STN showed distinctive, stereotypic periods of oscillatory burst discharge that lasted for 10–15 s (Fig. 1a). Intraburst firing rates reached several hundred spikes per second, and the bursts oscillated at low frequencies. Between bursts, STN units were either silent or fired irregularly at low rates. The burst activity of STN units was phase-locked and synchronized with other STN and GPe units (Fig. 1b, c), showing that it reflects population activity across both nuclei. Spontaneous synchronized bursting occurred regularly every 1–2 min and with occasional shifts in main frequency (Fig. 1d).

Based on correlation analysis and frequency plots using continuous periods of spontaneous spiking (324 ± 135 s per neuron), about half of STN (83/181) and a third of GPe units (31/102) fired in oscillatory bursts with frequencies between 0.1 and 4 Hz (20 ms time resolution). Similarly, 61% of STN–STN (46/76), 44% of STN–GPe (33/75), and 23% of GP–GPe (4/17) neuronal pairs displayed synchronized oscillatory bursts in that frequency range.

The STN–GPe system showed clear preferences for particular frequencies during synchronized bursts. The relative power spectrum analysis revealed two main population frequencies at $f_{01} = 0.44$ Hz and $f_{02} = 0.79$ Hz, respectively (Fig. 2a). A third

* Present address: Unit of Neural Network Physiology, Laboratory of Systems Neuroscience, National Institute of Mental Health, Bldg 36 2D-30, Bethesda, Maryland 20892, USA.

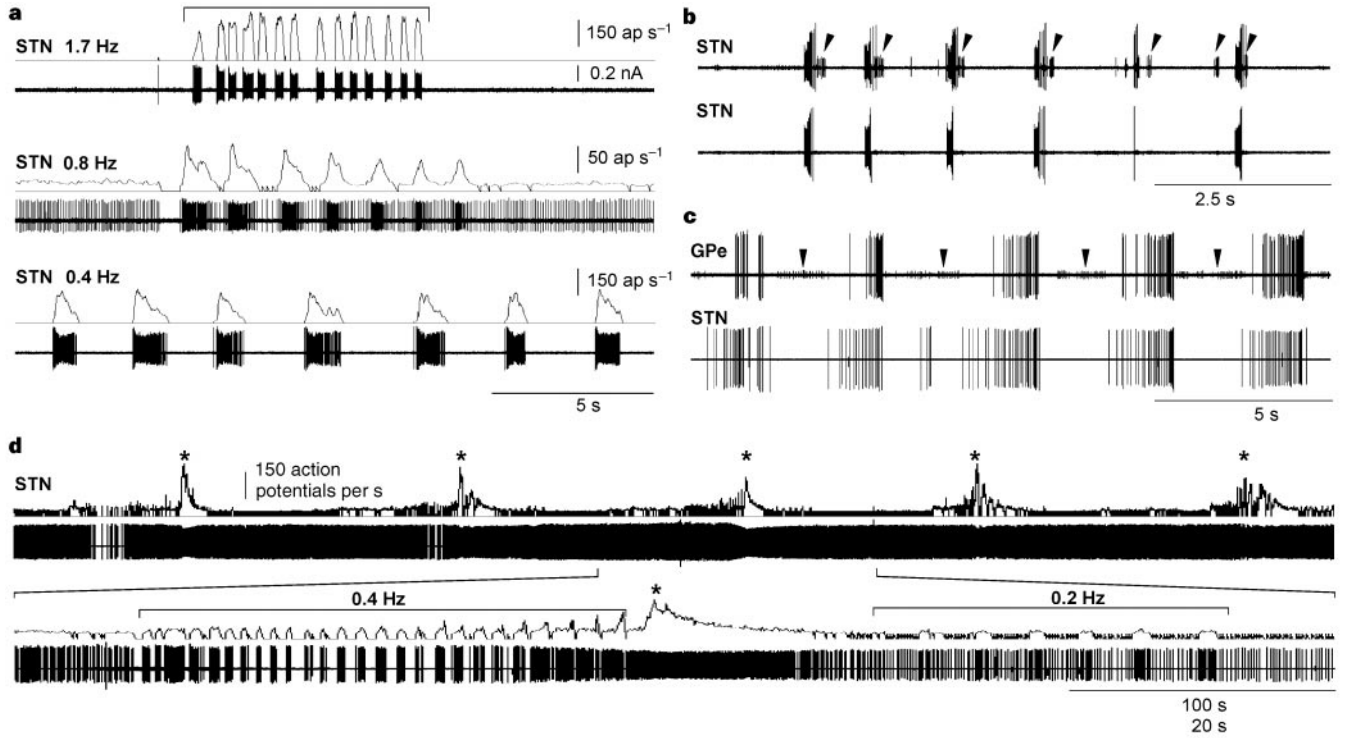

Figure 1 STN units display periods of oscillatory bursting, synchronized with other STN and GPe units. **a**, Oscillatory bursting periods with basic frequencies of 1.7, 0.8 and 0.4 Hz. Upper traces: instantaneous firing rates ($\tau = 0.1$ s). Lower traces: extracellular STN single-unit activity from different cultures. **b**, **c**, During synchronized bursting, STN units show stable phase relationships with other STN or GPe units at 0°, close to 0° (**b**, arrowheads), or 180° (**c**, arrowheads). Simultaneous extracellular multi-unit recording with two electrodes. **d**, Synchronized bursting periods are grouped regularly into longer periods of recurrent neuronal activity (1–2 min). During periods of synchronized bursting (asterisks), shifts in intraburst frequencies occasionally occur (brackets).

main frequency was found by plotting f_0 against the corresponding total relative power in the $f_0 \pm \Delta f$ range for each correlation function (Fig. 2b). The resulting probability distribution of f_0 peaked at the previously obtained frequencies $f_{01} = 0.42 \pm 0.09$ and $f_{02} = 0.82 \pm 0.11$, but also revealed a third dominant frequency at $f_{03} = 1.87 \pm 0.21$ Hz (gaussian fits, mean ± s.d.; Fig. 2c) with an eight-times smaller relative power than that of f_{01} and f_{02} (0.0029 ± 0.0001 vs. 0.022 ± 0.001; group threshold, 1.0 Hz). All main frequencies were found for STN, GPe and type f_0 correlation function (Fig. 2b, analysis of variance (ANOVA)). STN neurons fired in distinct phase-relation to other STN and GPe neurons during burst firing. Phase-locked bursting was observed at all main frequencies (Fig. 2d, ANOVA), and phases of minimum and maximum (Φ_{min},Φ_{max}) clustered mainly around (0°, ±180°) or (±180°, 0°) (Fig. 2e). These results characterize phase-locked oscillatory bursting as a synchronized network activity within the STN–GPe system that stabilizes at three discrete harmonic frequencies during which neurons either burst together or alternate in bursting.

Although both STN and GPe neurons engage in burst activity, a quantitative comparison of STN–STN and STN–GPe crosscorrelation functions showed that per single burst, STN units produced four times more spikes above expectation than GPe neurons (Fig. 2f).

The synchronized bursting was mainly confined to the low-frequency range. Using correlation analysis at higher time resolution (2 ms), oscillatory activity above 4 Hz was found in 12% of subthalamic (22/181) and 22% of pallidal (23/102) units. These oscillations were tightly correlated with a unit's average firing rate ($r_{STN} = 0.956$; $r_{GPe} = 0.998$) and were never found in the cross-correlation function (STN–STN, 0/73; STN–GPe, 0/76). Most units with these higher oscillations did not show synchronized oscillatory burst discharge (41/45). Thus, rhythmic firing at $f_0 > 4$ Hz probably reflected a neuron's intrinsic repetitive firing and not synchronized population activity.

In vivo, cortical stimulation produces complex sequences of excitation and inhibition in STN[12] and GPe[13] that also involve the corticostriatopallidal pathway. To test whether cortical input is necessary for synchronized bursting, the cortical culture was acutely isolated by a cut along the corticostriatal border (Fig. 3A). Despite a more than 50% reduction in spike activity in the STN (Fig. 3D), the cortical lesion did not abolish synchronized oscillatory bursting ($n = 5$ cultures, Fig. 3A–C). However, it centred the f_0 distribution at f_{02} (Fig. 3E), indicating that f_{02} is the preferred oscillatory state in the absence of afferent cortical drive. This experiment shows that synchronized bursting in the STN and GPe system is very robust, which was further supported by the finding that the average intraburst interspike interval did not change for STN units following cortical lesion (Fig. 3F). Cortical lesion did not change firing rates in the GPe. As striatal activity could also be important in synchronized bursting, striatal and cortical inputs were interrupted by a cut placed at the striatum–STN border. Under these conditions, synchronized bursting was still present ($n = 2$, data not shown).

In vivo, the main inhibitory input to the STN originates from the GPe[14], and the excitatory STN projects back to the GPe[15,16]. This feedback system is crucial for the generation of synchronized bursts. After projections between the STN and GPe were interrupted by a cut along the STN–GPe border ($n = 4$ cultures), the synchronized bursting was abolished (Fig. 3G, H) and STN unit firing became regular, as indicated by a more than 70% decrease in the coefficient of variance ($P < 0.005$; Fig. 3I). Also, the average firing rates of STN neurons increased slightly (13 ± 2 Hz intact vs 16 ± 2 Hz lesioned), and most STN units (13/20) intrinsically oscillated ($r = 0.96$, f_0 vs average firing rate) with no correlation in the crosscorrelation fucntion (13/13). Within 1 h after the lesion, long-lasting and uncorrelated burst activity built up in the STN (Fig. 3J). Spontaneous activity was almost absent in the isolated GPe (data not shown). These results show that the GPe is crucial for the generation

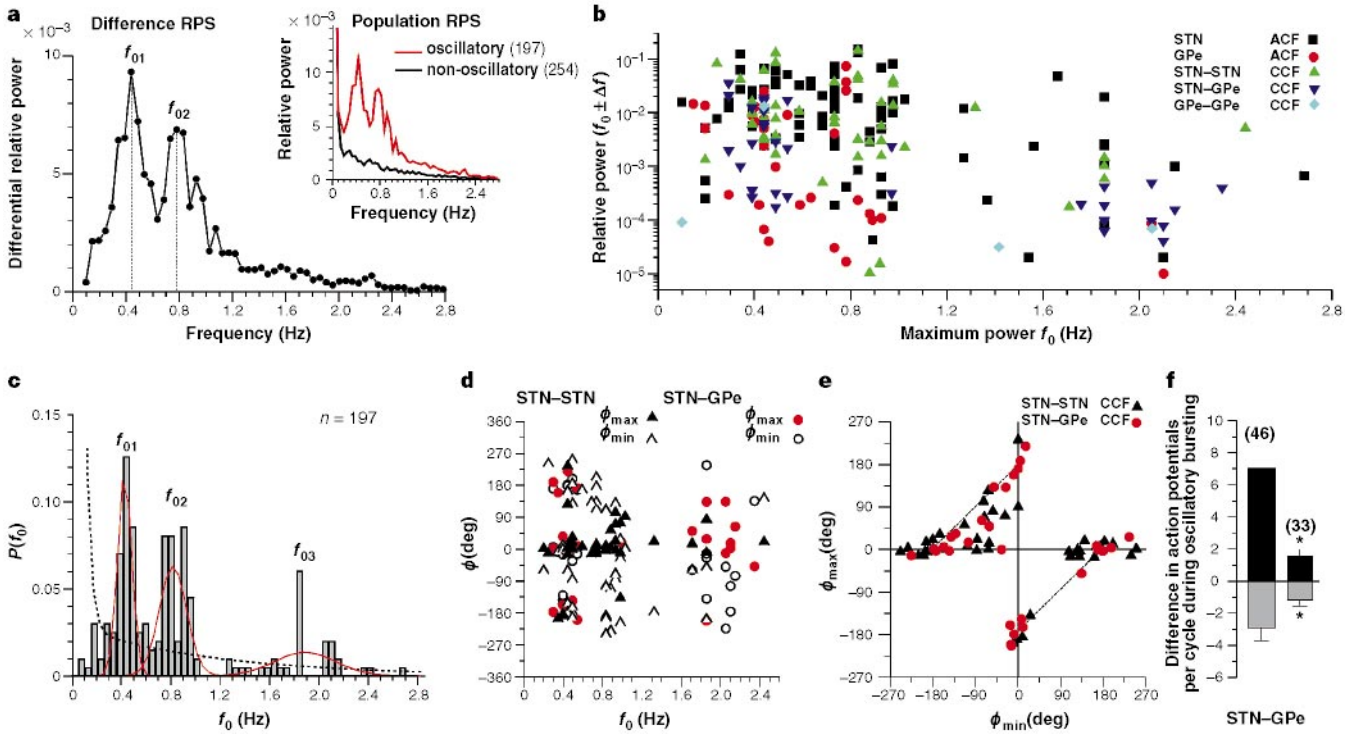

Figure 2 Quantitative analysis of synchronized oscillatory bursting in the STN and GPe. **a**, The difference relative power spectrum (RPS) reveals the tendency for bursting to occur at two main frequencies ($f_{01} = 0.44$ Hz, $f_{02} = 0.79$ Hz). Inset: average RPS from non-oscillatory (black) and oscillatory (red) auto- and cross-correlation functions (ACF and CCF, respectively). **b**, Scatter plot of f_0 versus relative power ($f_0 \pm \Delta f$) for each oscillatory correlation function and RPS. **c**, The probability distribution for f_0 [$P(f_0)$] obtained from **b** reveals three main population frequencies at $f_{01} = 0.42 \pm 0.09$, $f_{02} = 0.82 \pm 0.11$ and $f_{03} = 1.87 \pm 0.21$ (gaussian fit; red lines). Black dotted line indicates $P(f_0)$ for non-oscillatory cases (second-order exponential decay fit). **d**, Phase-locked firing between STN and GPe units is independent of f_0. **e**, Most units fire either synchronously at 0° or antiphasically at 180° with other STN and GPe units as revealed by the scatter plot of (ϕ_{min}, ϕ_{max}). Dashed lines indicate the expectation under the assumptions of symmetric burst–pause periods and equal distribution of all possible phases. **f**, STN units contribute significantly more spikes above chance ($\alpha_{0.995}$) than GPe units during one period of synchronized bursting ($P < 0.005$). Similarly, pauses lack significantly more spikes in STN neurons than in GPe neurons ($P < 0.05$).

of synchronized bursting and pallidal inputs are primarily responsible for the temporal organization of STN activity, rather than for the control of average firing rates of STN neurons.

Pharmacological studies support our model. Synchronized firing was blocked by bath application of the glutamate antagonist 6,7-dinitroquinoxaline-2,3-dione (DNQX) ($n = 3$ cultures, $n = 7$ neurons; Fig. 4a). Furthermore, STN burst activity elicited by local glutamate application to the STN initiated synchronized oscillatory bursting ($n = 5$; Fig. 4b). These results indicate that glutamatergic burst transmission from the STN to GPe is necessary for synchronized oscillatory bursting.

In addition, synchronized GABA (γ-aminobutyric acid) inputs to the STN, mimicked by local GABA application to the STN, elicited synchronized bursting that was preceded by a rebound burst in STN neurons ($n = 4$, Fig. 4c). This response profile indicates that synchronized inhibitory pallidal bursts could trigger synchronized oscillatory bursting by recruiting STN rebound bursts. The essential requirement of burst transmission between STN and GPe neurons for generating synchronized oscillatory activity was further supported by intracellular recordings from STN neurons combined with extracellular recordings in the GPe. Recordings were performed in cortex–STN–GPe triple cultures to exclude inhibitory inputs from the striatum. The data showed that pallidal bursts preceded hyperpolarizing, inhibitory potentials in STN neurons that were followed by rebound bursts ($n = 3$; Fig. 4d). These rebound bursts probably reflected intrinsic membrane properties of STN neurons, as rebound spiking could also be elicited by hyperpolarizing current injection into the cell bodies of cultured STN neurons (12/14; Fig. 4e)[17,18]. Finally, in cortex–striatum–STN cultures without GPe, spontaneous activity in the STN was characterized by long-lasting intermittent bursts (Fig. 4f) similar to those found in quadruple cultures after 1 h of acute GPe lesion.

The synchronized oscillatory bursting described here *in vitro* is very similar to activity patterns seen *in vivo* in the STN and GPe. In paralysed[19] and anaesthetized rats (M. Bevan, personal communication), oscillatory burst discharge in the low-frequency range was found in the STN and GPe. In primates, most GPe neurons fire in periods of several hundred milliseconds of high-frequency discharge, interspaced with similarly long-lasting silent periods[20–22]. These similarities at the neuronal activity level and the mature morphology of cortex–striatum–STN–GPe cultures[11] lead us to conclude that the synchronized oscillatory bursting described here captures a major activity pattern observed *in vivo*.

Our study identifies the STN–GPe system as a central pacemaker of the basal ganglia and should have far-reaching implications for basal ganglia function and dysfunction. First, in the culture system, the GPe was crucial for the temporal organization of STN activity, and GPe excitation was dictated by the STN. On the other hand, oscillatory bursts were less often encountered in the GPe than in the STN, and the burst strength of GPe units was less than that of STN units. This indicates that a few GPe neurons can have considerable control over the generation of synchronized oscillatory bursting within a small range of pallidal activity. As synchronized oscillatory burst discharge *per se* does not require cortical or striatal inputs, striatal inhibition of external pallidal neurons should allow for independent and very effective afferent control of the STN–GPe pacemaker.

Second, electrophysiological[5,19,23,24] and *in situ* hybridization[25] results from animal models of Parkinson's disease have indicated

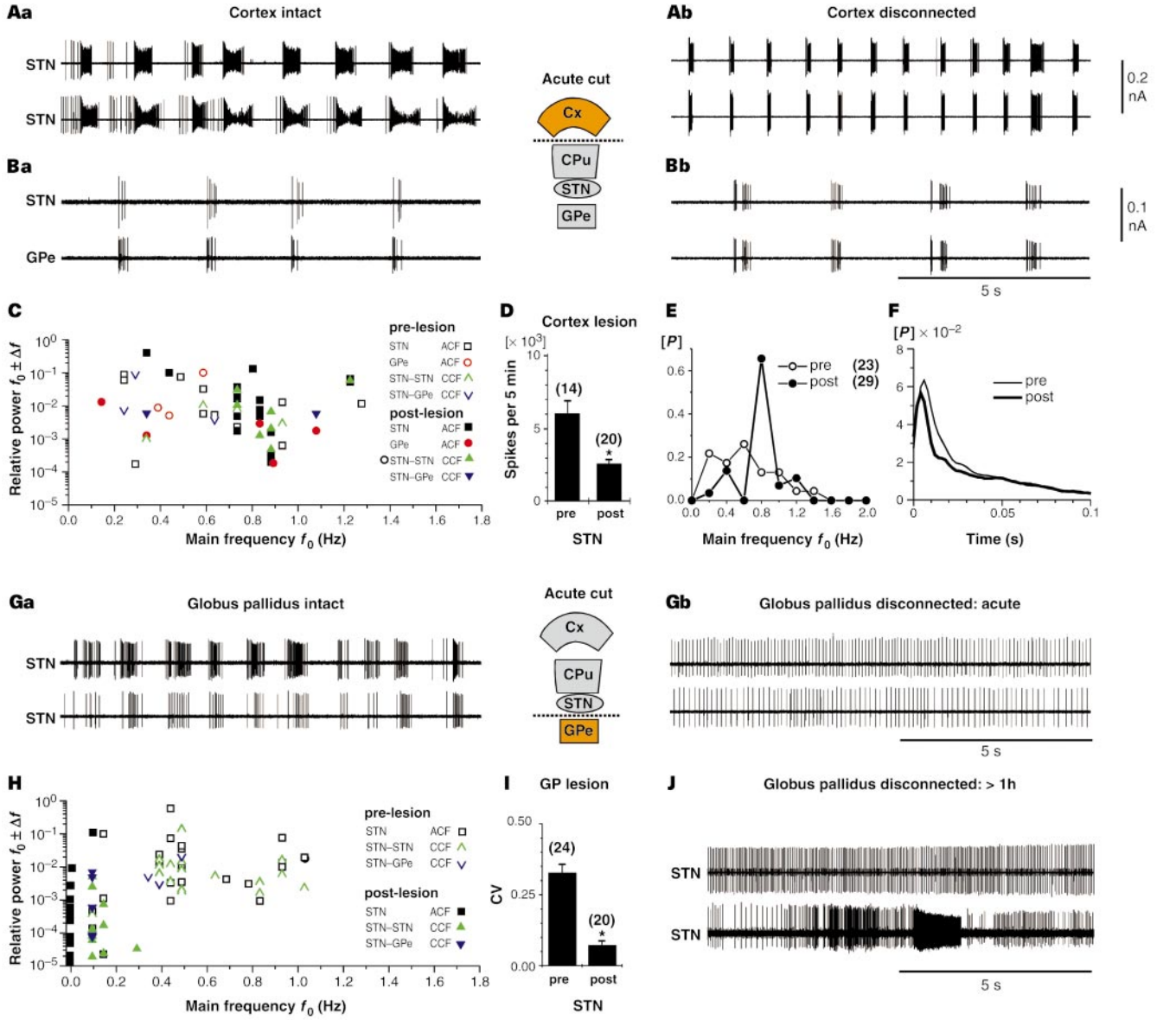

Figure 3 Synchronized oscillatory bursting does not depend on cortical input but on intact STN–GPe connectivity. **A**, **B**, The bursting does not depend on cortical inputs. Simultaneous recordings from different pairs of units in STN and GPe before (**Aa**, **Ba**) and after (**Ab**, **Bb**) cortical lesions. **C**, Scatter plot of f_0 and relative power in the $f_0 \pm \Delta f$ band before (pre-lesion, open symbols) and after (post-lesion, closed symbols) cortical inputs, synchronized bursting occurs predominantly at $f_{02} = 0.8$ Hz. **F**, The average intraburst interspike interval histogram for STN units does not change after cortical lesion. **G**, Acute pallidal lesion abolishes synchronized bursting in STN. Simultaneous recordings from different pairs of units before (**Ga**) and after (**Gb**) pallidal lesion. **H**, Scatter plot of f_0 and relative power in the $f_0 \pm \Delta f$ band before (pre-lesion, open symbols) and after (post-lesion, closed symbols) pallidal lesion. **I**, Reduction in coefficient of variance (CV) of STN firing after acute pallidal lesion. **J**, Simultaneous recording from STN units that display non-synchronized, non-oscillatory burst discharge after prolonged pallidal lesion (>1 h). Cx, cortex; CPu, striatum.

that the temporal properties of STN activity[2,5,25] and synchronization of neuronal activity in STN target nuclei[9,10] might be important for basal ganglia dysfunction resulting from striatal dopamine deficiency. Our results provide a basic mechanism by which synchronized oscillatory activity in the STN–GPe pacemaker could be linked to dopamine deficiency in the striatum. We suggest that dopamine, by acting on the 'indirect' striatopallidal pathway[3], controls the recruitment of STN and GPe neurons that become synchronized during pacemaker activity.

Finally, dopamine inputs were not present in the cortex–striatum–STN–GPe cultures. Thus, our *in vitro* system might more closely resemble a dopamine-deficient basal ganglia system rather than normal *in vivo* basal ganglia activity. This view is supported by the finding that dopamine depletion increases burst activity in the STN[5,23,24], external pallidum[21,26] and basal ganglia output nuclei[21,27]. Nevertheless, the highly synchronized oscillatory firing might only be the simplest detectable mode of the STN–GPe pacemaker, given widespread synchronization in both nuclei and possible entrained activity in STN target nuclei. Under normal conditions, we would envisage pacemaker activity in multiple STN–GPe feedback loops that attain dynamic phase relationships with each other and are individually controlled by striatal inhibition. As the STN–GPe pacemaker is in the 'indirect' pathway of the basal ganglia[3,15], the activity in striatal neurons that constitute the 'indirect' pathway might be qualitatively different from striatal activity in the 'direct' pathway that has been directly linked to movement execution[28,29]. The 'indirect' striatopallidal pathway would control temporal sequences of 'windows' through which activity in the 'direct' striatopallidal pathway is integrated by the output nuclei of the basal ganglia. □

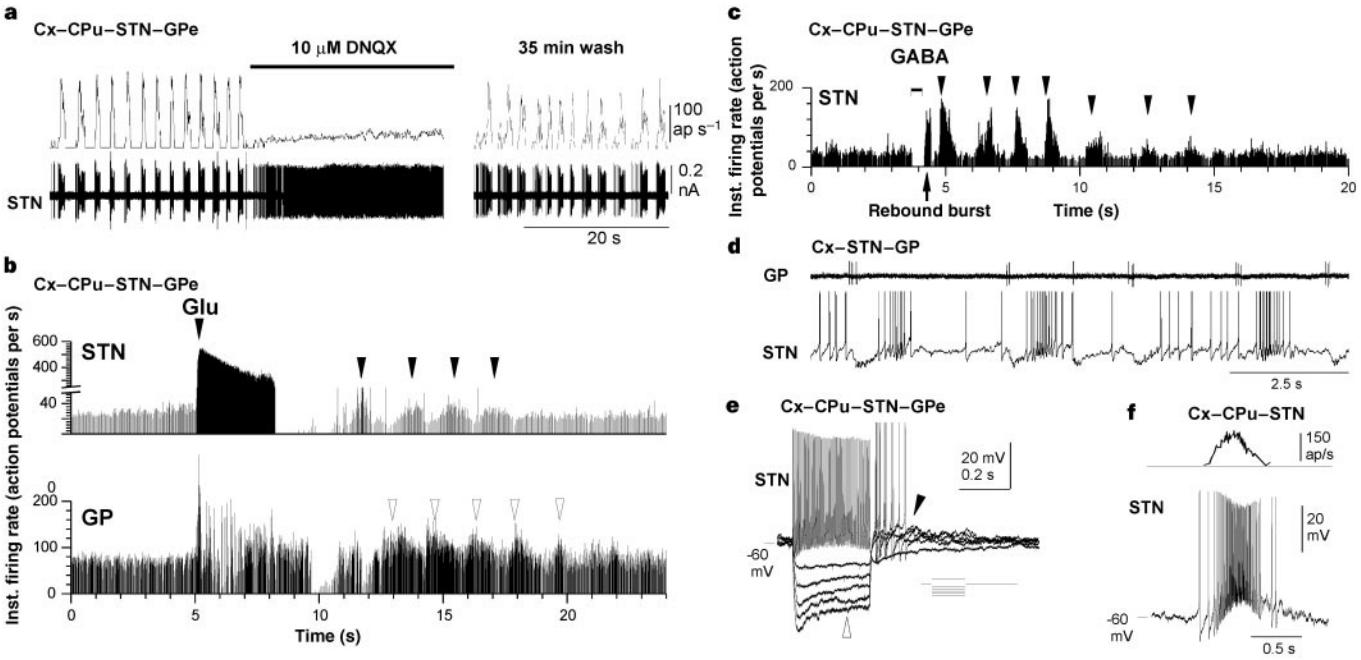

Figure 4 The mechanism of synchronized oscillatory burst generation in the STN–GPe pacemaker. **a**, Synchronized bursting is abolished by bath application of the glutamate antagonist DNQX. **b**, Synchronized oscillatory bursting can be elicited by local glutamate ejection (Glu) to the STN (200 ms, 1 mM). Instantaneous spike frequency plot for a simultaneously recorded STN and GPe unit. Note antiphasic bursting in STN and GPe (filled and open arrowheads). **c**, Local GABA application to the STN (200 ms, 1 mM) stops firing (bracket) and initiates oscillatory bursting (arrowheads) that is preceded by a rebound burst (arrow). **d**, During synchronized oscillatory bursting, GPe bursts precede a sequence of hyperpolarization and rebound burst excitation in STN neurons. **e**, Cultured STN neurons show weakly adapting high-frequency discharge, inward rectification (open arrowhead) and rebound excitation (filled arrowhead) upon steady-state current injections (inset). Average of 3.8 spikes per rebound response. **f**, Spontaneous long-lasting depolarization in STN neurons cultured without GPe (sharp intracellular recording).

Methods

Preparation of cultures. From coronal sections of rat brains at postnatal day 0–2 (Sprague-Dawley Harlan), dissected areas containing cortical, striatal, subthalamic and pallidal tissue were cultured in sequential order using a modified 'rollertube' technique[11]. The STN and GPe could be clearly identified in the mature culture during recording.

Electrophysiology. The extracellular solution contained (in mM) 126 NaCl, 0.3 NaH_2PO_4, 2.5 KCl, 0.3 KH_2PO_4, 1.6 $CaCl_2$, 1.0 $MgCl_2$, 0.4 $MgSO_4$. 26.2 $NaHCO_3$, and 11 D-glucose, saturated with 95% O_2 and 5% CO_2 (artificial cerebrospinal fluid; ACSF) warmed to 36.5 ± 1 °C. Extracellular recordings were obtained with patch electrodes filled with ACSF in current-follower mode, positioned under visual control. Intracellular recordings were obtained with sharp microelectrodes (110–150 MΩ) containing 2 M potassium acetate and 2% neurobiotin (Vector). Signals were recorded in Spike2 (Cambridge Electronic Design Ltd) and spike discharge was detected off-line using logic threshold operations or spike-template matching. Extracellular spike amplitudes and waveforms did vary during synchronized bursting (Figs 1, 3). Thus, to ensure proper single unit isolation, most units were isolated using a threshold operation and large signal-to-noise ratio (~6–10:1). Our data set mainly comprised single-unit activity.

Data analysis. Correlation functions were calculated for each unit at 2 and 20 ms time resolution (1,024 bins; ±1.024 s and ±10.24 s, respectively), smoothed (Fourier filter, quadratic function, cut off at 10 and 100 Hz), and normalized to average firing rates with confidence intervals ($\alpha_{0.005}$, $\alpha_{0.995}$) based on Poisson statistics using mean firing rates[30]. The relative power spectrum (RPS) was obtained by fast Fourier transformation of correlation functions (Mathematica) and normalization to the DC component. A single neuron or pair of neurons were considered oscillatory if the correlation function crossed at least twice the upper and lower confidence levels of multiple periods corresponding to the inverse of the main frequency $f_0 \pm 2\Delta f$ taken from the RPS. A peak detection algorithm was used to find the maximum peak in each RPS that defined the main frequency $f_0 > 0.08$ Hz for each oscillatory and non-oscillatory correlation function. We obtained the difference population RPS by subtracting the average RPS of all non-oscillatory units from that of oscillatory units. The phases of maximum (ϕ_{max}) and minimum (ϕ_{min}) indicate the time-to-maximum or time-to-minimum normalized to f_0^{-1} in crosscorrelation functions. Relative burst strength was calculated by integrating the area above or below expectation ($\alpha_{0.005}$, $\alpha_{0.995}$) during the burst oscillation period f_0^{-1} around time zero in STN–STN and STN–GPe crosscorrelation functions. Data are expressed as mean ± s.e.m. For statistical analysis, a factorial ANOVA with a *post hoc* Student–Newman–Keuls test (Statview) or Mann–Whitney *U*-test were used (significance level, $P < 0.05$). Correlation was estimated by linear regression analysis.

Pharmacology and anatomical reconstruction. GABA (1 mM), glutamate (1 mM; all Sigma), and DNQX (RBI) were dissolved in ACSF and either bath-applied or locally pressure-ejected close to the cell body of the neuron from which was being recorded. Acute cortical and pallidal lesions were performed with a micro-scalpel attached to a micromanipulator under visual guidance, after which new recordings were established. Lesion success was controlled for by the disappearance of evoked responses in the STN upon cortical or pallidal stimulation (tungsten stimulation electrode, 50 μs duration, 80–120 μA current amplitude). For each culture, we used parvalbumin immunohistochemistry[11] to verify recording and lesion positions anatomically.

Received 22 March; accepted 1 June 1999.

1. Matsumura, M. Kojima, J., Gardiner, T. W. & Hikosaka, O. Visual and oculomotor functions of the monkey subthalamic nucleus. *J. Neurophysiol.* **67,** 1615–1632 (1992).
2. Wichmann, T., Bergman, H. & DeLong, M. R. The primate subthalamic nucleus. I. Functional properties in intact animals. *J. Neurophysiol.* **72,** 494–506 (1994).
3. Albin, R. L., Young, A. B. & Penney, J. B. The functional anatomy of basal ganglia disorders. *Trends Neurosci.* **12,** 366–375 (1989).
4. Wichmann, T. & DeLong, M. R. Functional and pathophysiological models of the basal ganglia. *Curr. Opin. Neurobiol.* **6,** 751–758 (1989).
5. Bergman, H., Wichmann, T., Karmon, B. & DeLong, M. R. The primate subthalamic nucleus. II. Neuronal activity in the MPTP model of parkinsonism. *J. Neurophysiol.* **72,** 507–520 (1994).
6. Bergman, H., Wichmann, T. & DeLong, M. R. Reversal of experimental parkinsonism by lesions of the subthalamic nucleus. *Science* **249,** 1436–1438 (1990).
7. Limousin, P. *et al.* Electrical stimulation of the subthalamic nucleus in advanced Parkinson's disease. *N. Engl. J. Med.* **339,** 1105–1111 (1998).
8. Rodriguez, M. C. *et al.* The subthalamic nucleus and tremor in Parkinson's disease. *Mov. Disord.* **13,** 111–118 (1998).

9. Nini, A., Feingold, A., Slovin, H. & Bergman, H. Neurons in the globus pallidus do not show correlated activity in the normal monkey, but phase-locked oscillations appear in the MPTP model of Parkinson. *J. Neurophysiol.* **74,** 1800–1805 (1995).
10. Hurtado, J. M., Gray, C. M., Tamas, L. B. & Sigvardt, K. A. Dynamics of tremor-related oscillations in the human globus pallidus: A single case study. *Proc. Natl Acad. Sci. USA* **96,** 1674–1679 (1999).
11. Plenz, D., Herrera-Marschitz, M. & Kitai, S. T. Morphological organization of the globus pallidus–subthalamic nucleus system studied in organotypic cultures. *J. Comp. Neurol.* **397,** 437–457 (1998).
12. Kitai, S. T. & Deniau, J. M. Cortical inputs to the subthalamus: intracellular analysis. *Brain Res.* **214,** 411–415 (1981).
13. Kita, H. Responses of globus pallidus neurons to cortical stimulation: intracellular study in the rat. *Brain Res.* **589,** 84–90 (1992).
14. Kita, H., Chang, H. T. & Kitai, S. T. Pallidal inputs to subthalamus: intracellular analysis. *Brain Res.* **264,** 255–265 (1983).
15. Parent, A. & Hazrati, L. N. Functional anatomy of the basal ganglia. II. The place of the subthalamic nucleus and external pallidum in basal ganglia circuitry. *Brain Res. Rev.* **20,** 128–154 (1995).
16. Shink, E., Bevan, M. D., Bolam, J. P. & Smith, Y. The subthalamic nucleus and the external pallidum: two tightly interconnected structures that control the output of the basal ganglia in the monkey. *Neuroscience* **73,** 335–357 (1996).
17. Nakanishi, H., Kita, H. & Kitai, S. T. Electrical membrane properties of rat subthalamic neurons in an *in vitro* slice preparation. *Brain. Res.* **437,** 35–44 (1987).
18. Beurrier, C., Congar, P., Bioulac, B. & Hammond, C. Subthalamic nucleus neurons switch from single-spike activity to burst firing mode. *J. Neurosci.* **15,** 599–609 (1999).
19. Ruskin, D. N. *et al.* Multisecond oscillations in firing rate in the basal ganglia: Robust modulation by dopamine receptor activation and anaesthesia. *J. Neurophysiol.* **81,** 2046–2055 (1999).
20. DeLong, M. R. Activity of pallidal neurons during movement. *J. Neurophysiol.* **34,** 414–427 (1971).
21. Filion, M. Effects of the interruption of the nigrostriatal pathway and of dopaminergic agents on the spontaneous activity of globus pallidus neurons in the awake monkey. *Brain Res.* **178,** 425–441 (1978).
22. Aldridge, J. W. & Gilman, S. The temporal structure of spike trains in the primate basal ganglia: Afferent regulation of bursting demonstrated with precentral cerebral cortical ablation. *Brain Res.* **543,** 123–138 (1991).
23. Hollerman, J. R. & Grace, A. A. Subthalamic nucleus cell firing in the 6-OHDA-treated rat: basal activity and resonse to haloperidol. *Brain Res.* **590,** 291–299 (1992).
24. Hassani, O.-K., Mouroux, M. & Féger, J. Increased subthalamic neuronal activity after nigral dopaminergic lesion independent of disinhibition via the globus pallidus. *Neurosci.* **72,** 105–115 (1996).
25. Chesselet, M. F. & Delfs, J. M. Basal ganglia and movement disorders: an update. *Trends Neurosci.* **10,** 417–422 (1996).
26. Pan, H. S. & Walters, J. R. Unilateral lesion of the nigrostriatal pathway decreases the firing rate and alters the firing pattern of globus pallidus neurons in the rat. *Synapse* **2,** 650–656 (1988).
27. Miller, W. C. & DeLong, M. R. in *The Basal Ganglia II* (eds Carpenter, M. B. & Jayaraman, A.) 415–427 (Plenum, New York, 1987).
28. Wurtz, R. H. & Hikosaka, O. Role of the basal ganglia in the initiation of saccadic eye movements. *Prog. Brain Res.* **64,** 175–190 (1986).
29. Chevalier, G. & Deniau, J. M. Disinhibition as a basic process in the expression of striatal functions. *Trends Neurosci.* **13,** 277–280 (1990).
30. Abeles, M. Quantification, smoothing, and confidence limits for single-units' histograms. *J. Neurosci. Methods* **5,** 317–325 (1982).

Acknowledgements. We thank B. Teng for technical assistance with the preparation of cultures and for immunohistochemistry, and H. Steiner for discussions. This work was supported by grants from the National Parkinson Foundation (to D.P.) and the NINDS (to D.P. and S.T.K.).

Correspondence and requests for materials should be addressed to D.P. (e-mail: dplenz@codon.nih.gov).

Continued RAG expression in late stages of B cell development and no apparent re-induction after immunization

Wong Yu*†, Hitoshi Nagaoka*†‡, Mila Jankovic*§, Ziva Misulovin*‡, Heikyung Suh*‡, Antonius Rolink‖, Fritz Melchers‖, Eric Meffre*‡ & Michel C. Nussenzweig*‡

* *Laboratory of Molecular Immunology, and the ‡ Howard Hughes Medical Institute, the Rockefeller University, 1230 York Avenue, New York, New York 10021, USA*

§ *Institute for Molecular Genetics and Genetic Engineering, Vojvode Stepe 444A, Belgrade, Yugoslavia*

‖ *Basel Institute for Immunology, Grenzacherstrasse 487, Postfach, CH-4005 Basel, Switzerland*

† *These authors contributed equally to this work.*

Models of B-cell development in the immune system suggest that only those immature B cells in the bone marrow that undergo receptor editing express *V(D)J*-recombination-activating genes (RAGs)[1–3]. Here we investigate the regulation of *RAG* expression in transgenic mice carrying a bacterial artificial chromosome that encodes a green fluorescent protein reporter instead of RAG2 (ref. 4). We find that the reporter is expressed in all immature B cells in the bone marrow and spleen. Endogenous RAG messenger RNA is expressed in immature B cells in bone marrow and spleen and decreases by two orders of magnitude as they acquire higher levels of surface immunoglobulin M (IgM). Once *RAG* expression is stopped it is not re-induced during immune responses. Our findings may help to reconcile a series of apparently contradictory observations, and suggest a new model for the mechanisms that regulate allelic exclusion, receptor editing and tolerance.

To investigate the regulation of *RAG* expression, we produced transgenic mice that carry bacterial artificial chromosomes (BACs) modified by homologous recombination to encode a green fluorescent protein (GFP) reporter instead of RAG2 (ref. 4) (Fig. 1a). Three independently derived strains of NG-BAC transgenic mice were analysed and found to be identical in terms of GFP expression.

To determine whether GFP expression in B cells in NG-BAC transgenic mice reflects documented patterns of *RAG* expression, we examined bone-marrow cells by using multi-parameter flow cytometry. $B220^{-}CD43^{-}$ non-B cells and early precursors not known to express RAGs did not express GFP[3] (Fig. 1b, G1). In contrast, a high level of GFP expression was found in $B220^{+}CD43^{+}$ pro-B cells and a lower level was found in $B220^{low}CD43^{-}$ pre-B cells (Fig. 1b, G2 and G3, and Fig. 1c). Consistent with previous studies of RAG messenger RNA and protein expression in pre-B cells[3], GFP expression was lower in large $B220^{low}CD43^{-}$ IgM^{-} pre-B cells than in small pre-B cells (Fig. 1c). The finding that GFP fluorescence reflects RAG2 protein expression in small and large pre-B cells indicates that GFP is appropriately modulated in these cells despite the absence in GFP of amino-acid sequences that influence RAG2 stability[5]. Finally, mature $B220^{high}CD43^{-}$ B cells that re-circulate through the bone marrow did not express significant levels of GFP (Fig. 1b, G4). We conclude that the expression of GFP, like that of RAG2, is specifically induced in pro-B cells, decreases with the pre-B-cell transition, varies between large and small pre-B cells, and is turned off in mature B cells.

Immature B cells can be distinguished from earlier precursors in the bone marrow and from mature re-circulating bone marrow B cells because they are $Ig\kappa^{+}B220^{low}HSA^{high}$ (ref. 6). We found that all $Ig\kappa^{+}$ and $B220^{low}$ or HSA^{high} bone-marrow B cells are also GFP^{+}, whereas $GFP^{-}Ig\kappa^{+}$ B cells display a $B220^{high}$ and HSA^{low} phenotype consistent with mature re-circulating B cells (Fig. 1d). Thus, immature B cells in the bone marrow uniformly express the RAG2–GFP reporter but at a lower level than pro- and pre-B cells (Fig. 1c, d)

To determine whether immature B cells continue to express the GFP indicator after leaving the bone marrow, we analysed splenic B cells from NG-BAC transgenic mice. We found that 5–30% of all $B220^{+}$ cells or 2–12% of all lymphocytes are GFP^{+} (Fig. 2a). Mice that are 3–4 weeks old, have higher proportions of GFP^{+} B cells than older mice 6–24 weeks old (not shown). The GFP^{+} B cells in the spleen are IgM^{+} and either $Ig\kappa^{+}$ or $Ig\lambda^{+}$, so they are not contaminating B-cell precursors (Fig. 2a and data not shown). To determine whether the GFP^{+} B cells in the spleen are transitional B cells, we analysed spleen cells from NG-BAC transgenic mice using a combination of anti-B220, -HSA and 493 antibodies[6,7]. The antigen recognized by the 493 antibody is expressed on transitional but not mature B cells in the spleen[7]. Transitional B cells ($B220^{low}HSA^{high}493^{+}$) are uniformly GFP^{+}, whereas all mature B cells ($B220^{high}HSA^{low}493^{-}$) are GFP^{-} (Fig. 2b, c).

To determine whether GFP expression in immature and transitional B cells correlates with endogenous RAG expression we assayed for these mRNAs in B cells from non-transgenic mice. Consistent with our observations in GFP transgenic mice, mature B cells from wild-type mice do not express RAG1 or RAG2 mRNA or RAG2 protein (Fig. 3a, b). In contrast, immature B cells from bone marrow and spleen contain RAG1 and RAG2 but the level of RAG mRNA in these cells decreases by two orders of magnitude as they